Vol. 64: 123–140, 2015
doi: 10.3354/cr01304

CLIMATE RESEARCH
Clim Res

Published online July 7

# Transient high-resolution regional climate simulation for Greece over the period 1960–2100: evaluation and future projections

**P. Zanis[1,*], E. Katragkou[1], C. Ntogras[1], G. Marougianni[2], A. Tsikerdekis[1], H. Feidas[1], E. Anadranistakis[3], D. Melas[2]**

[1]Department of Meteorology and Climatology, School of Geology, Aristotle University of Thessaloniki, Thessaloniki, Greece
[2]Laboratory of Atmospheric Physics, School of Physics, Aristotle University of Thessaloniki, Thessaloniki, Greece
[3]Hellenic National Meteorological Service, Ellinikon, Greece

ABSTRACT: A transient regional climate model simulation with a spatial grid resolution of 10 km (RCM10), nested to a regional simulation with 25 km resolution (RCM25), was carried out over Greece with RegCM3 for the period 1960–2100 under the IPCC A1B scenario. RCM10 precipitation and temperature fields depict the finer regional characteristics over the complex Greek terrain compared to RCM25, but a station-based evaluation for the period 1975–2000 does not reveal a considerable improvement in RCM10 compared to RCM25. Future projections for the early-future period 2021–2050 indicate small changes, with annual temperature increasing mostly over land by less than 1.8°C and precipitation changing by ±15%, being mostly negative in the southern part of the domain. At the end of the century (2071–2100), the projected changes become larger, with mean annual temperature increasing by about 3.4 to 4.2°C over land and by 2.6 to 3.4°C over the sea and precipitation decreasing by 10 to 40%, with a positive gradient from the north to the south. Summer presents the largest future increase in mean near-surface temperature over the Greek mainland, while winter and spring show the largest decreases in precipitation rate. The number of hot days, warm nights, night frosts and continuous dry spell days and length of the growing season are projected to increase slightly in the near-future period, but markedly and consistently in the late 21st century future period in accordance with the generally warmer and drier climate projected from the RCM10 simulation.

KEY WORDS: Regional climate models · Greece · High resolution · Evaluation · Future projections



## 1. INTRODUCTION

Policy and decision makers in governmental and non-governmental organizations, as well as end-users in the private sector and the general public, require detailed regional information on future climate to assess the risks of anticipated climate changes due to the anthropogenic forcing of the greenhouse effect. Although high-resolution global climate models (GCMs) have been increasingly utilized over the last decade (Held & Zhao 2011), the recent simulations with GCMs used in the IPCC fifth assessment report (AR5) still have a coarse horizontal resolution to resolve the effects on regional climate of local- and regional-scale forcings, such as topographic characteristics with complex mountain ranges, coastlines, peninsulas, small islands and lakes, as well as land-use characteristics and chemical composition of short-lived species (e.g. aerosols, tropospheric ozone). Although planetary- and synoptic-scale forcings and circulations determine the statistics of weather events that characterize the cli-

*Corresponding author: zanis@geo.auth.gr

mate of a region, the above-mentioned regional- and local-scale forcings and circulations modulate the regional climate and can possibly provide feedback to the large-scale circulation (Giorgi & Mearns 1999, IPCC 2007).

Hence, regional climate models (RCMs) have been developed since the late 1980s for the application of dynamical downscaling methods to enhance the regional information provided by the GCMs for past and future climate simulations or by the large-scale reanalysis fields in hindcast simulations (Dickinson et al. 1989, Giorgi et al. 1990, Giorgi & Mearns 1999). Extensive application of the dynamical downscaling methodology with the use of RCMs has taken place over the last decade (e.g. Giorgi et al. 2004, Gao et al. 2006, Christensen & Christensen 2007, Déqué et al. 2007, Jacob et al. 2007, Sanchez-Gomez et al. 2009, Rauscher et al. 2010), and the capabilities and limitations of the methodology have been investigated (Giorgi & Mearns 1999, Laprise et al. 2008, Xue et al. 2014 and references therein).

The use of RCMs is necessary in regions with multiple topographic characteristics; Greece is a Mediterranean country characterized by complex topography, with steep orography from the mountainous regions to the coast, a long and convoluted coastline and many small islands in the Aegean and Ionian seas. Hence, the use of downscaling to higher resolution is necessary to assess the regional and subregional climate of the complex topographical area of Greece (Kostopoulou et al. 2007, Tolika et al. 2008, 2012, Zanis et al. 2009a). The highest commonly used horizontal resolution in multidecadal to centennial simulations with RCMs ranges between 50 and 25 km. But for mountainous regions, even 10 km, which is roughly the highest horizontal resolution limit regularly used in hydrostatic models, can be considered a coarse resolution (Im et al. 2010). Recently, a new high-resolution regional climate change ensemble with a horizontal resolution of 0.11° has been established for Europe within the World Climate Research Program Coordinated Regional Downscaling Experiment (EURO-CORDEX) initiative (Jacob et al. 2014).

Over the eastern Mediterranean (EM) region, climate conditions are characterized by moderate air temperatures and variable rainy weather during the winter season, often related to eastward movement of frontal systems (Maheras et al. 2001, Xoplaki et al. 2004). During spring, the mid-latitude baroclinicity zone moves northwards, and in summer, the region is subject to tropical influences leading to enhanced subsidence, which suppresses clouds and rain. This subsidence is primarily related to the interaction with the mid-latitude westerlies of an equatorially trapped Rossby wave to its west, induced by the South Asian monsoon heating, as well as an enhancement of the descent due to diabatic radiative cooling under clear sky conditions (Rodwell & Hoskins 1996, Tyrlis et al. 2013). Moreover, the geographic location of the Greek peninsula, with the contrasts of maritime and continental air masses, as well as its orographic features results in a distinctive climate variation from west to east and from north to south (Maheras & Anagnostopoulou 2003).

Furthermore, the whole Mediterranean is recognized among the most responsive regions to climate change (Giorgi 2006). Model projections based on GCMs and RCMs indicate a consistent warming and drying of the Mediterranean region mainly over the last decades of the 21st century for various emission scenarios (e.g. Gibelin & Déqué 2003, Gao et al. 2006, Diffenbaugh et al. 2007, Goubanova & Li 2007, Giorgi & Lionello 2008, Krichak et al. 2011, Lelieveld et al. 2013).

Most of the previous RCM studies for the future climate change of the EM or of specific countries of the EM were based on simulations with horizontal resolution down to 25 km. Projected climate change over the EM and Turkey has been analyzed by using a time-slice approach, with the reference (1961–1990) and future (2071–2100) climate simulations produced by RegCM3 with a horizontal resolution of 30 km under the IPCC A2 scenario (Önol & Semazzi 2009). They provided compelling evidence of the added value of RCM downscaling in the region based on countrywide averages of RegCM3 simulations being consistent with corresponding averaged station data. Krichak et al. (2011) carried out a double-resolution transient RCM climate change simulation experiment with RegCM3 over the period 1960–2060 under the IPCC A1B scenario for a near-coastal eastern zone of the EM region, with the inner domain having a horizontal resolution of 25 km. They revealed a notable sensitivity of the projected larger-scale climate change signals to the smaller-scale effects. Hadjinicolaou et al. (2011) assessed mid-21st century climate and weather extremes in Cyprus as projected by 6 RCMs with a horizontal resolution of 25 km under the IPCC A1B scenario, which indicated a shift in the mean climate to a warmer state, with a relatively strong increase in warm extremes. Lelieveld et al. (2013) presented similar model results from a transient simulation over the period 1950–2099 under the A1B scenario based on the RCM PRECIS with a horizontal resolution of ~25 km. Recently, Zittis et al.

(2014) studied the role of soil moisture in the amplification of climate warming in the EM based on a transient simulation with the Hadley Centre HadRM3P RCM covering the period 1951–2099 under the A1B scenario with a horizontal resolution of 25 km.

For Greece in particular, there are only a few studies so far on future climate change based on RCM simulations with spatial resolution down to 25 km. Zanis et al. (2009a) investigated the simulated changes in temperature and precipitation over Greece for the period 2071–2100 under the A2 emission scenario based on time-slice projections from 9 RCMs with a spatial grid resolution of 50 km carried out within the PRUDENCE project (http://prudence.dmi.dk/). An assessment of regional climate change for Greece based on available RCM simulations was presented by the Climate Change Impacts Study Committee (Zerefos et al. 2011). Tolika et al. (2012) updated the assessment of future climate change over Greece for summer and winter seasons using 22 simulations from various RCMs under the A2, A1B and B2 future emission scenarios of the IPCC. The study was based on time-slice projections with a spatial grid resolution of 50 km carried out within the PRUDENCE project and transient 21st century projections with a spatial resolution of 25 km carried out within the ENSEMBLES project. Nastos et al. (2013) studied future changes of aridity in Greece based on transient 21st century projections from 8 RCMs with a spatial resolution of ~25 km carried out within the ENSEMBLES project (www.ensembles-eu.org/).

Tselioudis et al. (2012) investigated whether the increased resolution of an RCM from 50 to 11 km introduces novel information in future precipitation change over the mountainous region of Greece. So far, this is the first study showing results of future climate change with such a high spatial resolution (of 11 km) for the region of Greece. However, the study was based only on two 5 yr runs, a control run (1991–1995) and a future climate run based on the IPCC A1B scenario (2091–2095). Furthermore, Önol (2012) presented for the first time a long-term high-resolution (of 10 km) regional climate simulation using RegCM3 for the EM including Greece, but this simulation was a hindcast simulation driven by NCEP reanalysis over the period 1961–2008. Here, we present results of a high-resolution simulation over the period 1960–2100 with RegCM3 that constitutes a transient regional projection for future climate change, for the first time to our knowledge, with 10 km spatial resolution for Greece.

## 2. DATA AND MODEL SETUP

The high-resolution (10 km grid resolution) transient regional climate simulation (1960–2100) was performed with the RCM RegCM3 over Greece (hereafter referred to as RCM10) with 143 × 109 grid cells horizontally, 18 vertical levels and the model top at 50 mb. The domain and the model topography are shown in Fig. 1. The RCM10 simulation was initialized in December 1958, with the first 2 yr of the simulation considered as the spin-up time. This high-resolution simulation was a nested run of the RegCM3 simulation with 25 km spatial resolution over an extended European domain carried out in the framework of the European Union project ENSEMBLES (hereafter referred to as RCM25). In our centennial RCM10 simulation case, the dynamical downscaling ratio was 2.5 to 1, down to the highest horizontal resolution limit regularly used in hydrostatic RCMs, thus reducing the gridbox surface from 625 to 100 km$^2$. In turn, the RCM25 simulation used lateral boundary conditions from the T63 GCM ECHAM5 coupled to the ocean model MPI-OM (run 3) with 1.875° resolution for the 20th century (Roeckner 2006) and the 21st century under the IPCC Special Report on Emissions Scenarios (SRES) A1B scenario (Roeckner 2008). The 20th century simulation (including year 2000) used observed anthropogenic forcings of carbon dioxide ($CO_2$), methane ($CH_4$), nitrous oxide ($N_2O$), chlorofluorocarbons (CFCs), ozone ($O_3$) and sulfate ($SO_4$). The A1B scenario is part of the A1 family, which describes a balance across all energy sources. The ECHAM5 experiment was initialized in year 2000 of the 20th

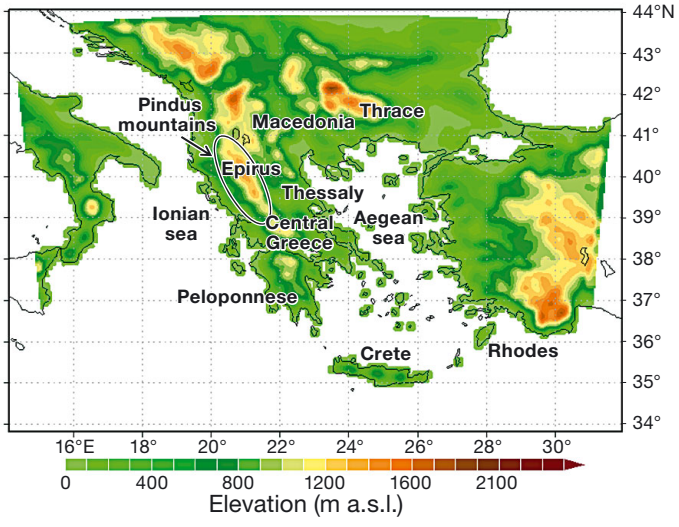


Fig. 1. Topography of the Greek domain with a grid horizontal resolution of 10 km. The regions of Greece are also indicated

century run and continues until year 2100 with anthropogenic forcings ($CO_2$, $CH_4$, $N_2O$, CFCs, $O_3$ and $SO_4^{2-}$) according to A1B. The A1B scenario predicts a medium-high increase of $CO_2$ concentration to about 700 ppm by 2100 (IPCC 2007). SRES scenarios have been used for the climate projections of the IPCC fourth assessment report (AR4). However, the recent climate projections in IPCC AR5 are based on the most recent representative concentration pathways (RCPs). Comparison of $CO_2$ concentrations for the 21st century from the RCPs and SRES scenarios shows that A1B lies between RCP6 and RCP8.5 but is closest to RCP6 (Meinshausen et al. 2011). Rogelj et al. (2012) also showed that the median of the projected warming for the end of the 21st century under the A1B scenario is found between the values of the RCP6 and RCP8.5 scenarios but nearer to RCP6.

RegCM3 was initially developed at the National Center for Atmospheric Research (NCAR), and has been used in a number of RCM in studies of regional climate and seasonal predictability around the world (Giorgi et al. 2006, Pal et al. 2007). The dynamical core is based on the hydrostatic version of the Pennsylvania State University/NCAR mesoscale model version 5 (Grell et al. 1994). The radiative transfer package is taken from the community climate model version 3 (Kiehl et al. 1996). The large-scale cloud and precipitation computations are performed by the subgrid explicit moisture scheme (Pal et al. 2000). The biosphere–atmosphere transfer scheme (Dickinson et al. 1993) is used to represent surface processes, while boundary layer physics is described via the non-local vertical diffusion scheme of Holtslag et al. (1990).

The RCM25 simulation over Europe, which provided the lateral boundary conditions for the RCM10 simulation, used the Grell scheme (Grell 1993) for convection, implementing the Fritsch & Chappell (1980) closure assumption (hereafter referred to as Grell-FC). However, a sensitivity study of RegCM3 to the convective scheme for southeastern Europe showed that a cold bias with Grell is significantly reduced when the Emanuel convective scheme (Emanuel & Živković-Rothman 1999) is used, even during months of low convective activity (Zanis et al. 2009b). Furthermore, in a previous study for central Europe with RegCM3, high-resolution simulations with the default Grell-FC scheme tend to significantly overestimate precipitation for the mountainous area of the Carpathians (Torma et al. 2011). Torma et al. (2011) thus suggested an adjustment of some parameters in the Grell-FC scheme to reduce precipitation in the nested simulation such as the cloud-to-rain autoconversion rate, raindrop evaporation rate coefficient and raindrop accretion rate. Furthermore, Önol (2012) carried out a high-resolution regional climate simulation (10 km) nested in a 50 km RegCM3 simulation with the default Grell-FC scheme for the EM, driven by NCEP reanalysis over the period 1961–2008. In this study, the nested high-resolution simulation reveals a clear overestimation of precipitation over the mountainous regions of Greece during winter and spring in comparison to gridded datasets (see Fig. 6).

Hence, it was necessary to configure the convection scheme to optimise RegCM3 for our high-resolution simulations over Greece. The model configuration was chosen after evaluating 6 yearly sensitivity simulations with different convection schemes, as described in more detail by Mystakidis et al. (2012). Specifically, the simulations comprised 2 experiments using the Grell-FC scheme and 4 experiments using the Emanuel convective scheme. The 2 simulations with the Grell-FC scheme included one simulation with the default version and the other simulation with the modification suggested by Torma et al. (2011). The 4 experiments with the Emanuel scheme include changes in the relaxation rate $a$ (kg m$^{-2}$ s$^{-1}$ K$^{-1}$), which determines the rate at which the cloud-base upward mass flux is relaxed to steady state, and in the warm cloud autoconversion threshold $l_0$ (kg kg$^{-1}$), which determines the amount of cloud water available for precipitation conversion, following the study by Segele et al. (2009).

Simulations using the modified Emanuel convective scheme with $l_0 = 0.01$ and $a = 0.1$ showed the best model performance, reducing the mean bias in temperature over 25%, in cloudiness over 20% and in precipitation over 70% when compared with the respective observed values from the network of the Hellenic National Meteorological Service (HNMS) (Mystakidis et al. 2012). Following these results, the high-resolution transient regional climate simulation (1960–2100) was performed using the Emanuel scheme with $l_0 = 0.01$ and $a = 0.1$.

The transient high-resolution simulation was evaluated over the period 1975–2000 using temperature and precipitation measurements from 79 stations of the HNMS observational network. Selection of the period 1975–2000 was based on optimum spatial coverage of stations over this period, meaning a compromise between the longest period and the highest density of stations. The data were subjected to a series of quality control tests including internal consistency checks and identification of outliers in the monthly values. An algorithm to correct for missing values,

based on current WMO guidelines, was also applied using the criterion that a year is considered to be complete when at least 8 monthly values are recorded (Marougianni et al. 2012). The evaluation analysis was done on a monthly basis; hence, monthly mean time-series of surface temperature and precipitation were extracted from model fields to be compared with the station observations. Because of differences between station altitude and model grid altitude, a correction was applied in modelled temperature, with a standard temperature vertical lapse rate of 6°C km$^{-1}$.

The metrics used for model evaluation are (1) the mean annual bias, providing an estimation of the over- or underestimation of the selected meteorological variable; (2) the correlation coefficient R of the observed and modeled time-series over the HNMS stations to identify their temporal agreement; and (3) the normalized standard deviation (NSD), which is the ratio of the standard deviation of the modeled monthly values to the standard deviation of the observed values. This measure ideally equals unity and becomes either >1 or <1 depending on whether the model over- or underestimates the amplitude of variability of the evaluated variable.

Furthermore, in our analysis, we used monthly temperature and precipitation from (1) the forcing T63 general circulation model (GCM) ECHAM5 coupled to MPI-OM (run 3) with 1.875° resolution for the 20th century (Roeckner 2006) downloaded from the Climate and Environmental Retrieval and Archive (CERA) database (http://cera-www.dkrz.de/CERA/index.html), (2) the RCM25 simulation over Europe and (3) the E-OBS gridded dataset based on observational data (Haylock et al. 2008) with a spatial resolution of 0.22° on a rotated grid (www.ecad.eu/).

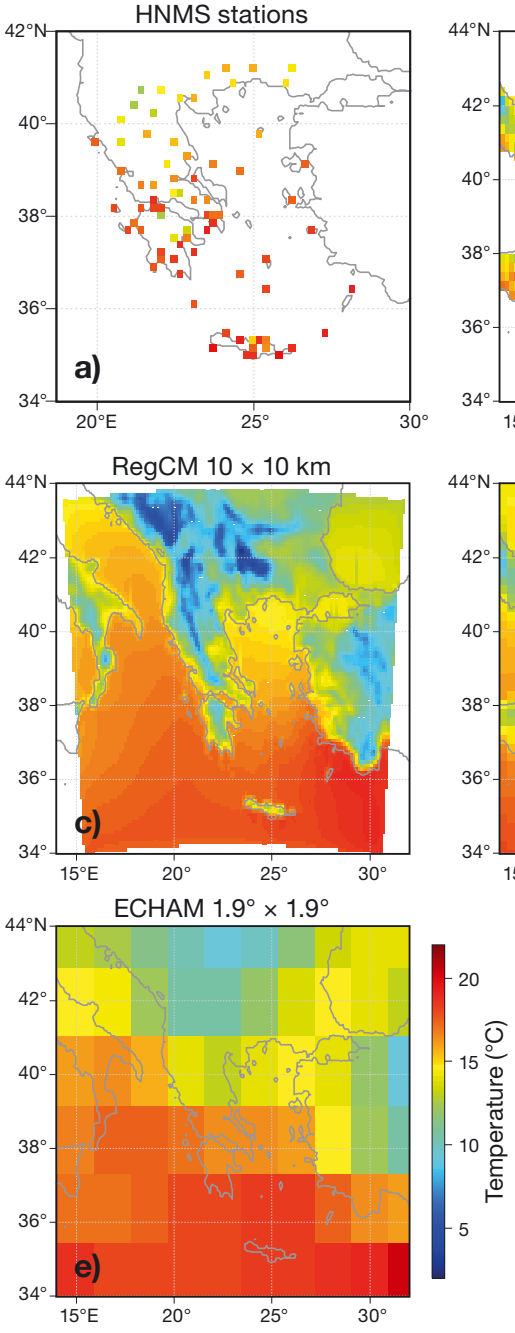


Fig. 2. Mean annual near-surface temperature (1975–2000) for (a) Hellenic National Meteorological Service (HNMS) stations, (b) E-OBS, (c) RCM10, (d) RCM25 and (e) the forcing GCM ECHAM5

## 3. RESULTS

### 3.1. Evaluation over the period 1975–2000

The average annual near-surface temperatures over the period 1975–2000 for the HNMS stations are shown as points in Fig. 2a, while the respective gridded E-OBS field is illustrated in Fig. 2b. Visual comparison of Fig. 2a,b indicates rather colder annual temperatures in E-OBS than at the HNMS stations. The annual near-surface temperature average fields for RCM10, RCM25 and ECHAM are also shown in Fig. 2 with their respective grid resolution. Visually, we note a rather good comparison of the RCM10 temperature field with RCM25 and E-OBS, with a tendency for colder tem-

peratures and more structural topographic characteristics over the mountainous regions (Pindus mountain range) due to the higher resolution. Fig. 2e also shows the limited regional information of the temperature field of the GCM in comparison to the E-OBS, RCM10 and RCM25 fields.

Similarly, Fig. 3 shows the annual precipitation sum over the period 1975–2000 for the HNMS stations, E-OBS gridded data, RCM10, RCM25 and the forcing GCM ECHAM5. Visually, we note a good comparison of the RCM10 precipitation field compared to RCM25, with RCM10 depicting the finer regional characteristics over the mountain regions. Both RCM10 and RCM25 capture the precipitation pattern shown in E-OBS, but there is a tendency for higher precipitation over western Greece and the Pindus mountain range in comparison to the E-OBS and HNMS stations. Fig. 3 also indicates the improvement in depicting spatially the topographic characteristics as we move from the global model with about 190 km resolution towards RCM25 and the even finer characteristics in RCM10.

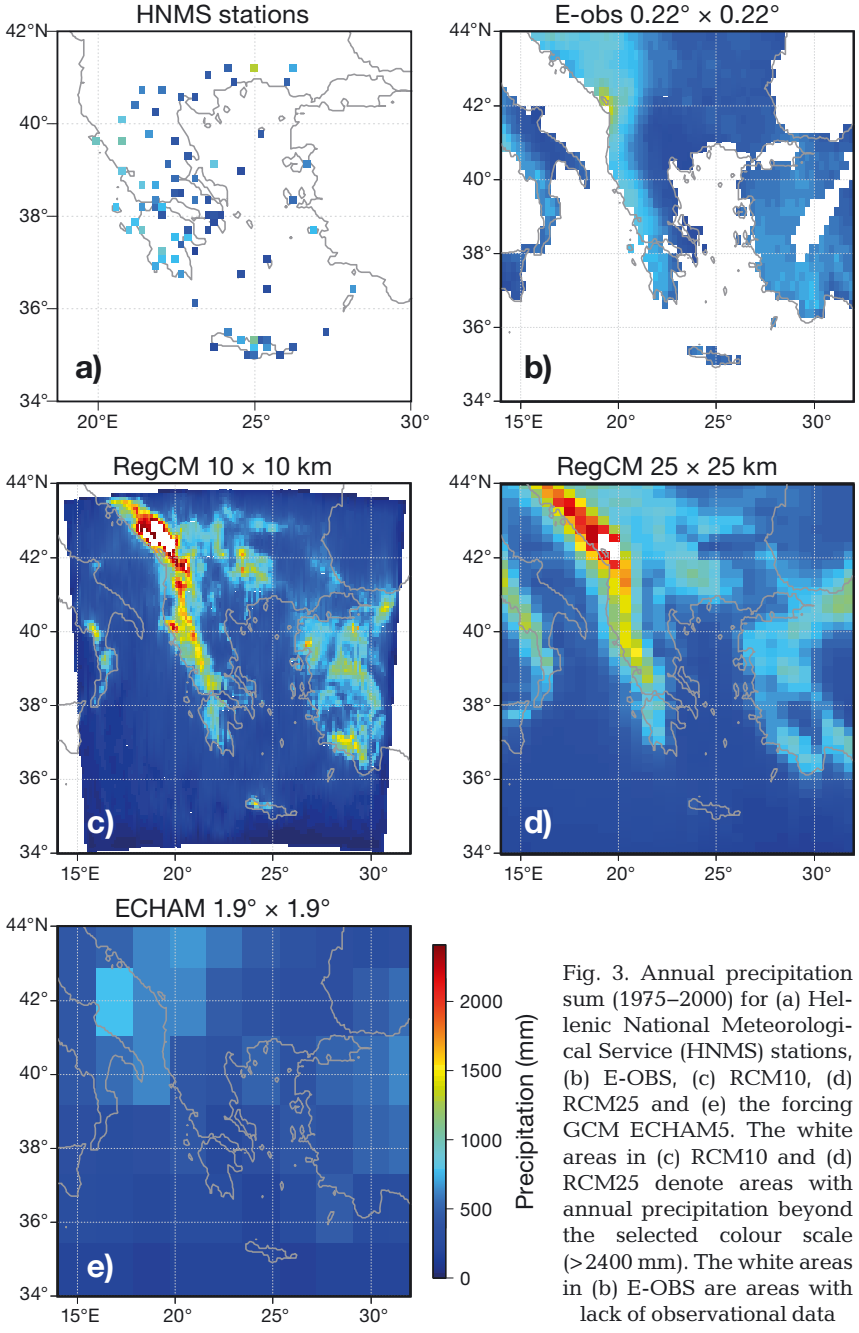


Fig. 3. Annual precipitation sum (1975–2000) for (a) Hellenic National Meteorological Service (HNMS) stations, (b) E-OBS, (c) RCM10, (d) RCM25 and (e) the forcing GCM ECHAM5. The white areas in (c) RCM10 and (d) RCM25 denote areas with annual precipitation beyond the selected colour scale (>2400 mm). The white areas in (b) E-OBS are areas with lack of observational data

Considering that the actual station data provide a more realistic basis for the evaluation of the RCM10 simulation, the statistical evaluation measures were calculated with regard to the HNMS station data. Fig. 4 and Table 1 provide a quantitative outlook for the evaluation of RCM10 and RCM25 with respect to HNMS stations on an annual basis. Specifically, Fig. 4 illustrates the mean annual surface temperature (top) and precipitation (bottom) bias of RCM10 and RCM25 for the time period 1975–2000. Furthermore, Table 1 shows summary statistics of the 3 evaluation metrics (bias, R, NSD) for near-surface temperature and precipitation. The results for near-surface temperature indicate negative biases for both RCM25 and RCM10. The median annual bias for all HNMS stations is slightly reduced in RCM10 (median bias −2.2°C) by about 0.3°C compared to RCM25 (median bias −2.5°C). The percentile analysis shows that the P75 (3rd quartile) of the bias is also reduced in RCM10 but that in the lower part of the distribution, the P25 (1st quartile) indicates slightly larger negative biases for RCM10 compared to RCM25. Furthermore, the maximum and minimum values of the biases are larger in RCM10 than in RCM25. A question that arises is to what extent the differences in the temperature biases of RCM10 and RCM25 are related to the different resolution or the different convective schemes. To address this issue, we carried out a sensitivity study running an additional annual simulation of RCM10 for 1 yr (year 1995) but using

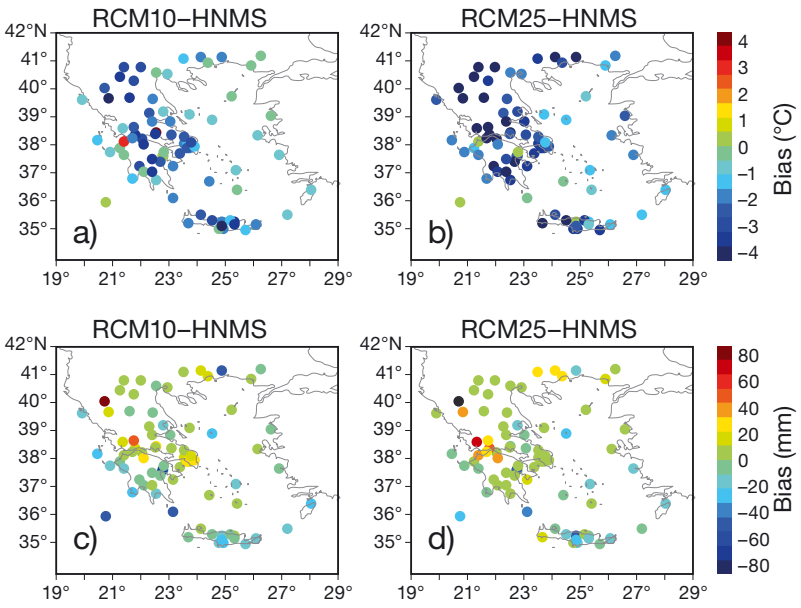


Fig. 4. Mean annual bias in near-surface temperature and precipitation over the period 1975–2000 for (a,c) RCM10 and (b,d) RCM25

Table 1. Summary statistics of the major evaluation metrics on an annual basis (25th, 50th and 75th percentiles [P25, P50 and P75, respectively] and mean, minimum and maximum values) based on the comparison of RCM10 and RCM25 near-surface temperature and annual precipitation values with the respective values from the 79 Hellenic National Meteorological Service stations. The statistical evaluation metrics include mean bias (°C for temperature, mm for precipitation), temporal correlation coefficient and normalised standard deviation (NSD)

| | Bias | | R | | NSD | |
|---|---|---|---|---|---|---|
| | RCM10 | RCM25 | RCM10 | RCM25 | RCM10 | RCM25 |
| **Near-surface temperature** | | | | | | |
| P25 | −3.23 | −2.99 | 0.94 | 0.94 | 0.77 | 0.89 |
| P50 | −2.18 | −2.46 | 0.95 | 0.95 | 0.84 | 0.95 |
| P75 | −1.20 | −1.70 | 0.95 | 0.95 | 0.91 | 1.02 |
| Mean | −2.49 | −2.42 | 0.95 | 0.94 | 0.84 | 0.97 |
| Minimum | −11.61 | −8.88 | 0.92 | 0.93 | 0.56 | 0.72 |
| Maximum | 2.87 | 1.43 | 0.96 | 0.95 | 1.15 | 1.33 |
| **Annual precipitation** | | | | | | |
| P25 | −24.05 | −15.39 | 0.29 | 0.24 | 0.68 | 0.63 |
| P50 | −9.83 | −3.26 | 0.35 | 0.33 | 0.92 | 0.80 |
| P75 | 7.35 | 4.22 | 0.43 | 0.41 | 1.32 | 0.96 |
| Mean | −8.27 | −2.83 | 0.34 | 0.32 | 0.99 | 0.91 |
| Minimum | −79.29 | −54.03 | 0.09 | 0.07 | 0.12 | 0.35 |
| Maximum | 70.07 | 86.86 | 0.52 | 0.52 | 3.48 | 3.73 |

the same convective scheme (Grell-FC) as in RCM25 (hereafter denoted RCM10G). A direct comparison of RCM10 using Emanuel with RCM10G using Grell-FC indicated a cold bias of RCM10G over the Greek domain ranging from −0.2 to −0.5°C (see Fig. S1 in the Supplement at www.int-res.com/articles/suppl/c064p123_supp.pdf). This result indicates that the reduction of the median annual bias in near-surface temperature by about 0.3°C for RCM10 compared to RCM25 is rather linked to the different convective schemes implemented through a feedback mechanism, as has been also discussed by Zanis et al. (2009b). Use of the Emanuel convective scheme imposes a stronger convective activity than the Grell-FC scheme, stronger vertical redistribution of humidity, fewer low-level clouds, more short-wave solar radiation absorbed from the ground and, hence, warmer low-level temperatures. However, the different resolutions in RCM10 and RCM25 play a role in the distribution of the biases.

In the case of precipitation, there is a larger negative bias in RCM10 than in RCM25, with the median bias being −9.8 mm for RCM10 and −3.3 mm for RCM25, but the distribution of biases is wider in RCM10 than in RCM25 (Table 1) based on the P25 and P75 values (1st and 3rd quartiles, respectively). However, RCM25 produces slightly more precipitation at the HNMS stations over the Pindus mountain range compared to RCM10. The Pindus mountain range stretches from near the Greek–Albanian borders in northern Epirus, entering the Epirus region and Macedonia region in northern Greece, down to the north of the Peloponnese. For 5 HNMS stations located in the greater area of the Pindus of northwestern Greece (Ioannina, Kastoria, Konitsa, Kozani and Florina), the mean annual precipitation bias in RCM10 is −19.9 ± 82.1 mm, while in RCM25, it is 29 ± 86 mm. A direct comparison of RCM10 using Emanuel with RCM10G using Grell-FC indicated a wet bias of RCM10G over western Greece and the Pindus mountain range from 50 to 300 mm annually (see Fig. S1 in the Supplement). These biases are higher than the difference of the annual precipitation bias between RCM10 and RCM25. This indicates that the use of Grell-FC in RCM25 leads to a slightly higher precipitation rate and bias than RCM10 (using

the modified Emanuel scheme), but these wet biases accentuate at higher resolution, as they become larger with the use of the Grell-FC scheme in RCM10G. A seasonal analysis of the biases in temperature and precipitation for the RCM10 simulation is provided in Table S1 in the Supplement at www.int-res.com/articles/suppl/c064p123_supp.pdf.

The temporal correlation of RCM10 with observations is high for temperature, ranging from 0.92 to 0.96 at all stations, but is considerably lower for precipitation, with values ranging from 0.09 to 0.52. Generally, climate models have difficulties successfully representing the amount of precipitation and its spatial and temporal characteristics since it is controlled by several factors including the convection scheme, the energy and water budget and topography. Table 1 indicates that the higher spatial resolution in RCM10 compared to RCM25 has no impact on the temporal correlations for temperature and precipitation. Furthermore, the spatial correlation is rather low for precipitation (ranging from 0.2 to 0.3) and higher for the homogeneous field of temperature (around 0.8) for both RCM10 and RCM25. This result indicates no considerable improvement in spatial correlation, despite the higher spatial resolution in RCM10 compared to RCM25, presumably because of the limited number of stations over the mountainous regions.

The NSD shows a median value of 0.84 in temperature and 0.92 in precipitation for RCM10, while the respective values for RCM25 are 0.95 and 0.8. This indicates that the amplitude of variability is slightly more underestimated in RCM10 than in RCM25 for temperature but reverses for precipitation. The range of the distribution in NSD values (difference between P25 and P75 in Table 1) are greater in RCM10 than in RCM25, which could be related to the different resolution.

As mentioned in Section 2, selection of the period 1975–2000 for our evaluation was based on optimum spatial coverage of stations over this period. Nevertheless, we carried out a similar analysis with fewer HNMS stations for the control period 1961–1990, revealing similar results with those discussed for the period 1975–2000.

### 3.2. Future projections in annual near-surface temperature and precipitation

The simulated RCM10 projected changes on an annual basis in near-surface temperature and precipitation between the 2 future time slices (2021–2050 and 2071–2100; hereafter FUT1 and FUT2, respectively) and the control time slice (1961–1990) are shown in Figs. 5 & 6. In the first half of the century, small changes are shown for temperature and precipitation. Mean annual temperature increases mostly by up to 1.4°C over most of Greece and by up to 1.8°C over parts of Peloponnese and Crete as well as islands of the Aegean Sea (Fig. 5a). The change in maximum annual temperature is slightly higher, with an increase ranging from 1.4 to 1.8°C over land for almost the whole of Greece (Fig. 5c). The change in minimum annual temperature is slightly lower, with an increase ranging from 1.0 to 1.4°C over the whole of Greece except the island of Rhodes, where the increase ranges from 1.4 to 1.8°C (Fig. 5e). All of these changes in temperature are statistically significant at the 95% confidence level. Concerning precipitation, the near-future change is ±15%, being mostly negative in the southern part of the domain, indicating drier conditions, but these changes are non-statistically significant at the 95% confidence level (Fig. 6a). The largest part of the changes in total precipitation are related to changes in non-convective precipitation (Fig. 6c,e).

At the end of the 21st century, larger changes in both near-surface temperature and precipitation are projected under the A1B scenario. Mean annual temperature increases by about 3.4 to 4.2°C over land and by 2.6 to 3.4°C over the sea (Fig. 5b). The change in maximum annual temperature is slightly higher, reaching values of about 4.2 to 4.6°C over the mainland (Fig. 5d), while the change in minimum annual temperature is slightly lower, with an increase up to 3.8°C over land (Fig. 5f). Precipitation is projected to decrease between 10 and 40%, with the stronger decrease shown over southern Greece (Fig. 6b). Here, we also note that the largest part of the changes in total precipitation are related to non-convective precipitation (Fig. 6d,f), namely decreasing significantly (at the 95% confidence level) all over Greece with stronger decreasing rates towards the southern parts (Fig. 6f).

Notably, RCM25 and RCM10 projected changes in near-surface temperature and total and convective precipitation (not shown) are comparable in magnitude and spatial distribution. This indicates the robustness of the climate change signal in the future projections, despite the different resolution and the different convective schemes implemented. Furthermore, this robustness, especially for the end of the 21st century, implies that the physical signal of climate change in both simulations is presumably greater than the important issue of the model's internal variability resulting from chaotic processes intrin-

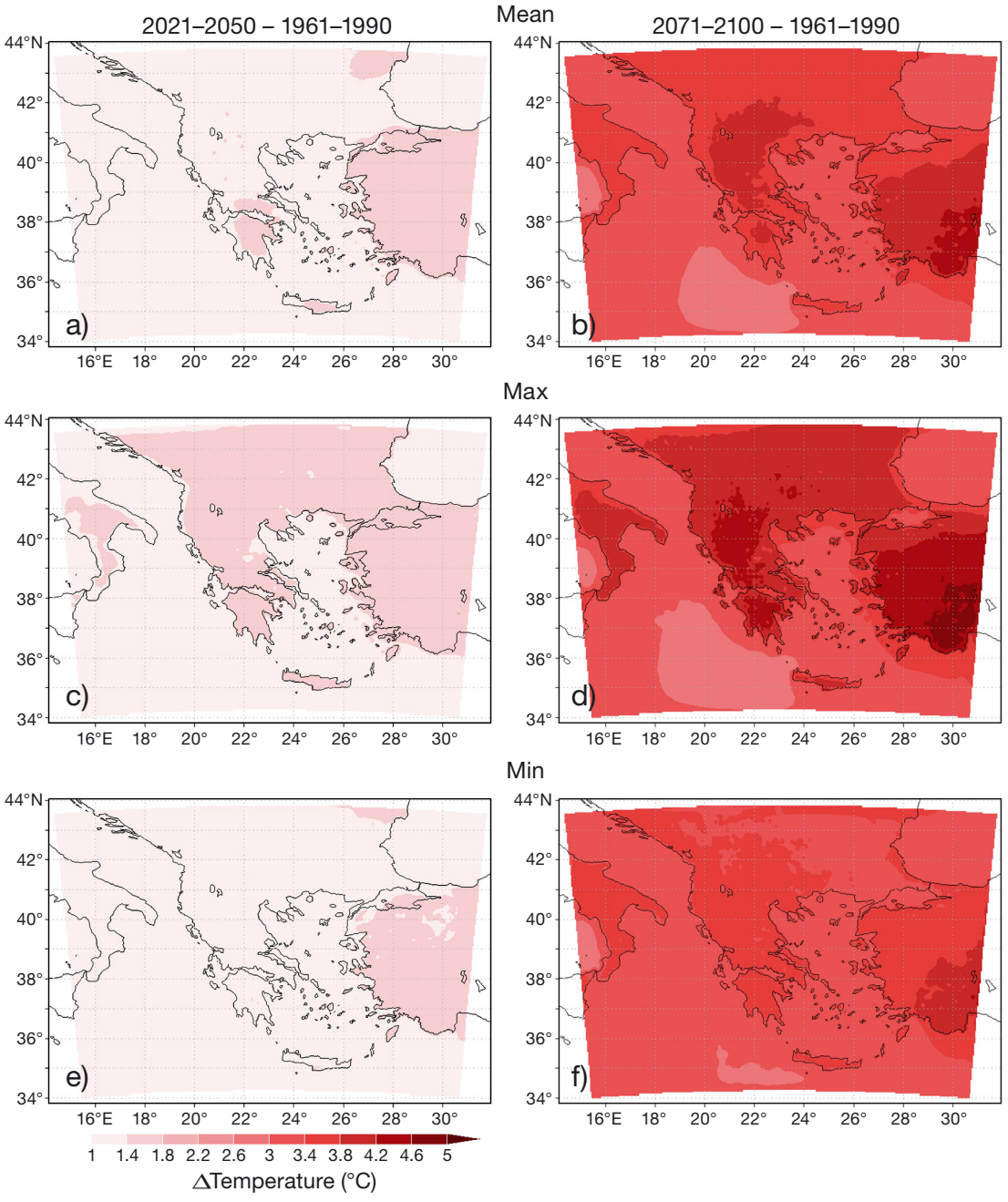


Fig. 5. Change between 2021–2050 and 1961–1990 as well as between 2071–2100 and 1961–1990 for (a,b) annual mean, (c,d) maximum near-surface temperature and (e,f) minimum near-surface temperature based on the high-resolution simulation RCM10. All differences are statistically significant at the 95% confidence level according to a 2-tailed paired *t*-test

sic to the atmosphere (Giorgi & Bi 2000, Crétat & Pohl 2012). The issue of model internal error is more of a concern for the early decades of the 21st century, when the physical signal of the anthropogenic climate change is low. However, this issue can only be addressed quantitatively by generating ensembles of simulations since, owing to its random nature, the variability should tend towards zero as the number of ensemble members increases (O'Brien et al. 2011).

### 3.3. Future projections in seasonal near-surface temperature and precipitation

The RCM10 projected changes on a seasonal basis in mean near-surface temperature and precipitation between 2071–2100 and the control period 1961–1990 are illustrated in Figs. 7 & 8. In winter, we note the lowest changes in mean near-surface temperature, with values ranging between 3.0 and 3.4°C over

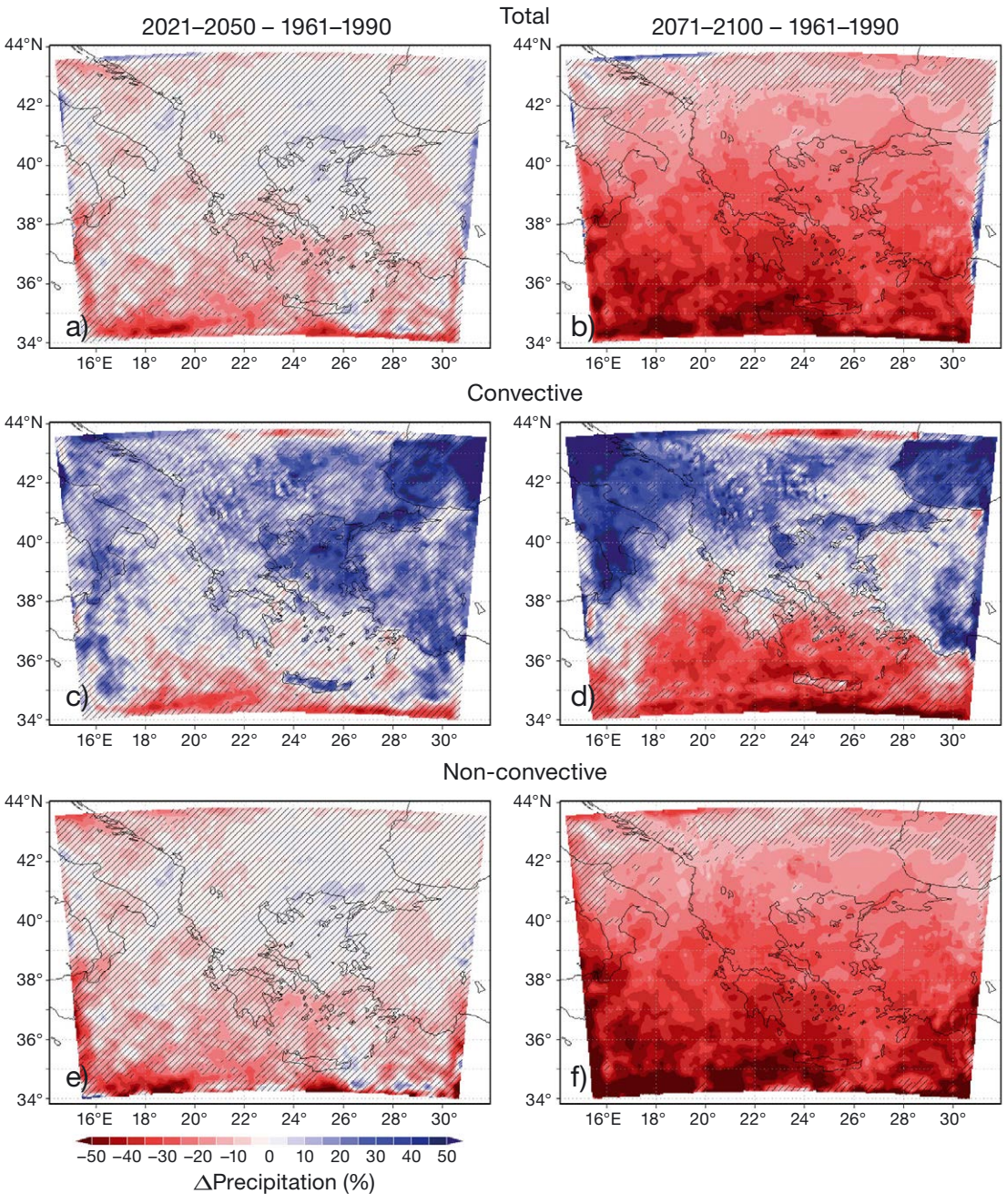


Fig. 6. Percentage change between 2021–2050 and 1961–1990 as well as between 2071–2100 and 1961–1990 for (a,b) annual total precipitation, (c,d) convective precipitation and (e,f) non-convective precipitation based on the high-resolution simulation RCM10. The line shading indicates areas in which the differences between future runs and the control run are not statistically significant at the 95% confidence level according to a 2-tailed paired *t*-test

land and the northern Aegean Sea (Fig. 7a). In spring, the changes over the largest part of the Greek mainland range between 3.4 and 3.8°C (Fig. 7b). In autumn, the changes are slightly higher, especially over northern Greece, the Peloponnese and Crete, with values ranging between 3.8 and 4.2°C (Fig. 7d). The largest changes in mean near-surface temperature are seen during summer over the Greek mainland, with values between 4.2 and 4.6°C for southern Greece (e.g. the Peloponnese, Crete and east central Greece), between 4.6 and 5°C for northeastern Greece and more than 5°C for northwestern Greece. Changes in maximum near-surface temperature in summer for FUT2, with values higher than 5°C, cover a larger part of northern Greece (not shown) in comparison to the mean summer temperature. For FUT1,

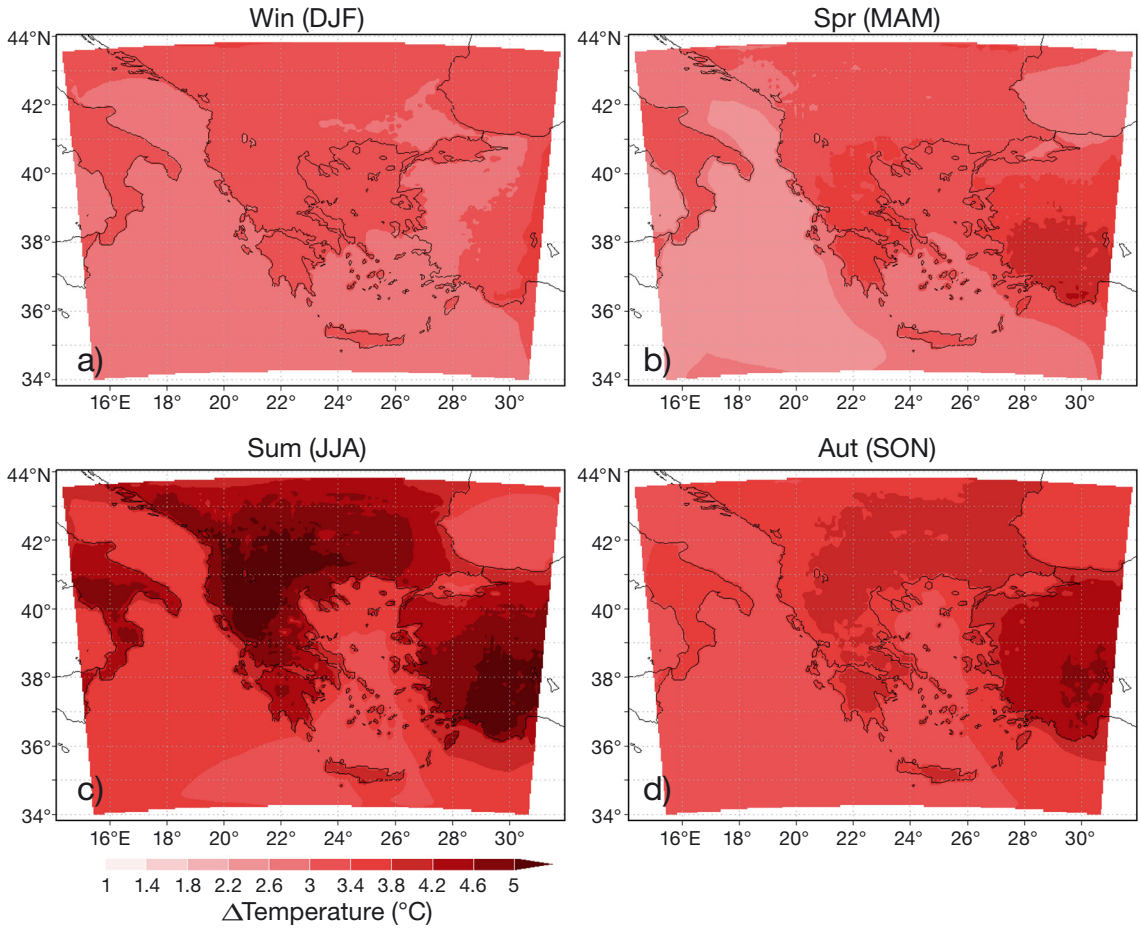


Fig. 7. Seasonal mean near-surface temperature change between 2071–2100 and 1961–1990 for (a) winter, (b) spring, (c) summer and (d) autumn based on the high-resolution RCM10. All differences are statistically significant at the 95 % confidence level according to a 2-tailed paired *t*-test

the summer period shows the largest changes throughout the year in mean near-surface temperature, with values ranging between 1.8 and 2.2°C over the land, while the winter period shows the lowest, with values ranging between 0.8 and 1.4°C (not shown).

Concerning precipitation for the FUT2 period, summer presents the lowest changes in the mean daily precipitation rate because of the very low amounts of precipitation during this season, with these changes being non-statistically significant at the 95 % confidence level (Fig. 8d). Winter and spring show the largest decreases in future precipitation daily rate, with values ranging from –0.15 mm $d^{-1}$ to more than –0.75 mm $d^{-1}$ over the Pindus mountain range. Winter shows the largest decreases in precipitation rate in western and southern Greece, while spring shows the largest decrease in northern Greece (Fig. 8a,b). The percentage changes in total precipitation reach a decrease up to roughly 40 to 45 % in certain regions during winter and spring (see Fig. S2 in the Supplement). Autumn also shows decreasing daily precipitation rates for the whole of Greece (Fig. 8d), but the changes are smaller compared to spring and winter. The largest part of the changes in total precipitation are related to changes in non-convective precipitation for all seasons. The changes in convective precipitation for the FUT2 period are provided in Fig. S3 in the Supplement.

In the FUT1 period, the seasonal changes in precipitation daily rate are either slightly positive or negative but generally non-statistically significant at the 95 % confidence level (not shown). For example, in winter, the daily precipitation rate decreases in southern Greece by about –0.15 to –0.45 mm $d^{-1}$ but increases over northern Greece by 0.15 to 0.30 mm $d^{-1}$. In spring, the precipitation daily rate slightly decreases by about –0.15 mm $d^{-1}$ for the whole of Greece, while in autumn, it increases by a similar amount for the whole of Greece.

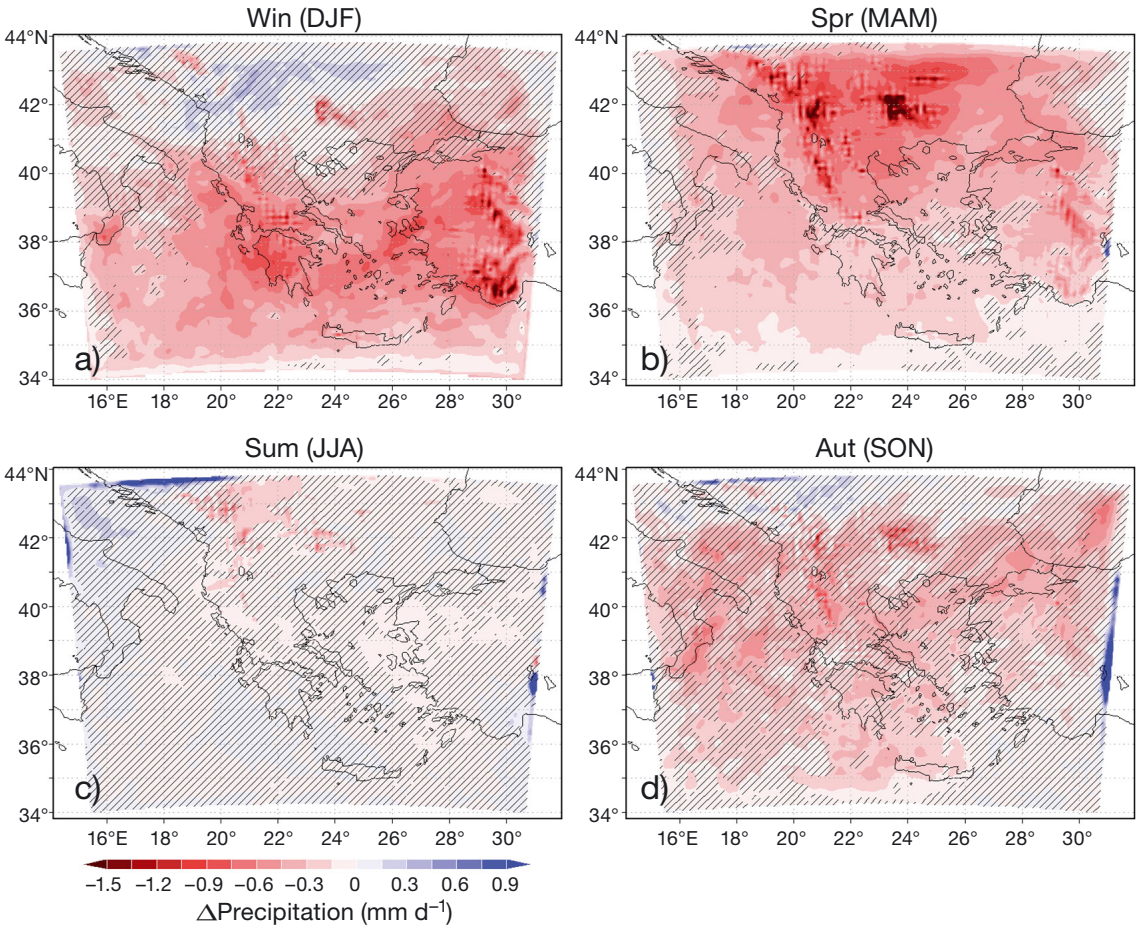


Fig. 8. Seasonal mean precipitation change between 2071–2100 and 1961–1990 for (a) winter, (b) spring, (c) summer and (d) autumn based on the high-resolution RCM10. The line shading indicates areas in which the differences between future runs and the control run are not statistically significant at the 95% confidence level according to a 2-tailed paired *t*-test

### 3.4. Future projections in climate indices

RCM10 simulations were used to calculate future changes in the FUT1 and FUT2 periods relative to the control period in climate indices including (1) the number of hot days with Tmax > 35°C; (2) the number of warm nights with Tmin > 20°C; (3) the number of night frost days with Tmin < 0°C; (4) the number of continuous dry spell days with daily precipitation < 1 mm; and (5) the length of the growing season, which corresponds to the number of days between the last spring frost and the first autumn frost. These indicative climate indices were selected following the assessment of regional climate change for Greece by the Climate Change Impacts Study Committee (Zerefos et al. 2011).

For the FUT1 period, an increase in annual hot days is projected, with Tmax > 35°C on the order of 14 to 21 d for most of Greece except in Peloponnese, where the increase is slightly higher, ranging between 21 and 28 d (Fig. 9a). For the FUT2 period, we note larger increases in the number of hot days, ranging between 49 and 56 d for most of Greece, with the largest increases in the range of 56 to 63 d in southwestern Peloponnese (Fig. 9b). The number of warm nights with Tmin > 20°C is projected to increase by roughly 10 to 30 d in the FUT1 period (Fig. 9c) and by about 50 to 80 d in the FUT2 period (Fig. 9d), with the largest increases seen over southern Greece (Peloponnese and Crete).

Concerning the number of night frost days, RCM10 simulations in the FUT1 period project a decrease in the range of 4 to 8 d for southern Greece and a slightly higher decrease in northern Greece, between 8 and 12 d (Fig. 9e). The latitudinal distinction in the decrease of night frost days becomes stronger in the FUT2 period, when decreases are projected in the range of 20 to 28 d for northern Greece, 12 to 20 d

in central Greece and 4 to 16 d in southern Greece (Fig. 9f). The larger decrease in night frost days over northern Greece is linked to the generally higher temperatures and the lower possibility for the development of night frosts. The changes in the number of hot days, warm nights and night frosts are statistically significant at the 95% confidence level according to a 2-tailed paired *t*-test for all grid points for both the FUT1 and FUT2 periods.

The growing season is also projected to extend by about 4 to 16 d in the FUT1 period and by about 20 to 40 d in the FUT2 period, with the largest increases in northern Greece (Fig. 10c,d). For the island of Crete, no change in night frost days or growing season is projected for both the FUT1 and FUT2 periods, because of the generally higher temperatures throughout the year. All of the above-mentioned changes in hot days, warm nights, night frost days and length of the growing season for both the FUT1 and FUT2 periods are consistent with the generally warmer climate projected for the A1B IPCC scenario, as discussed in Section 3.3.

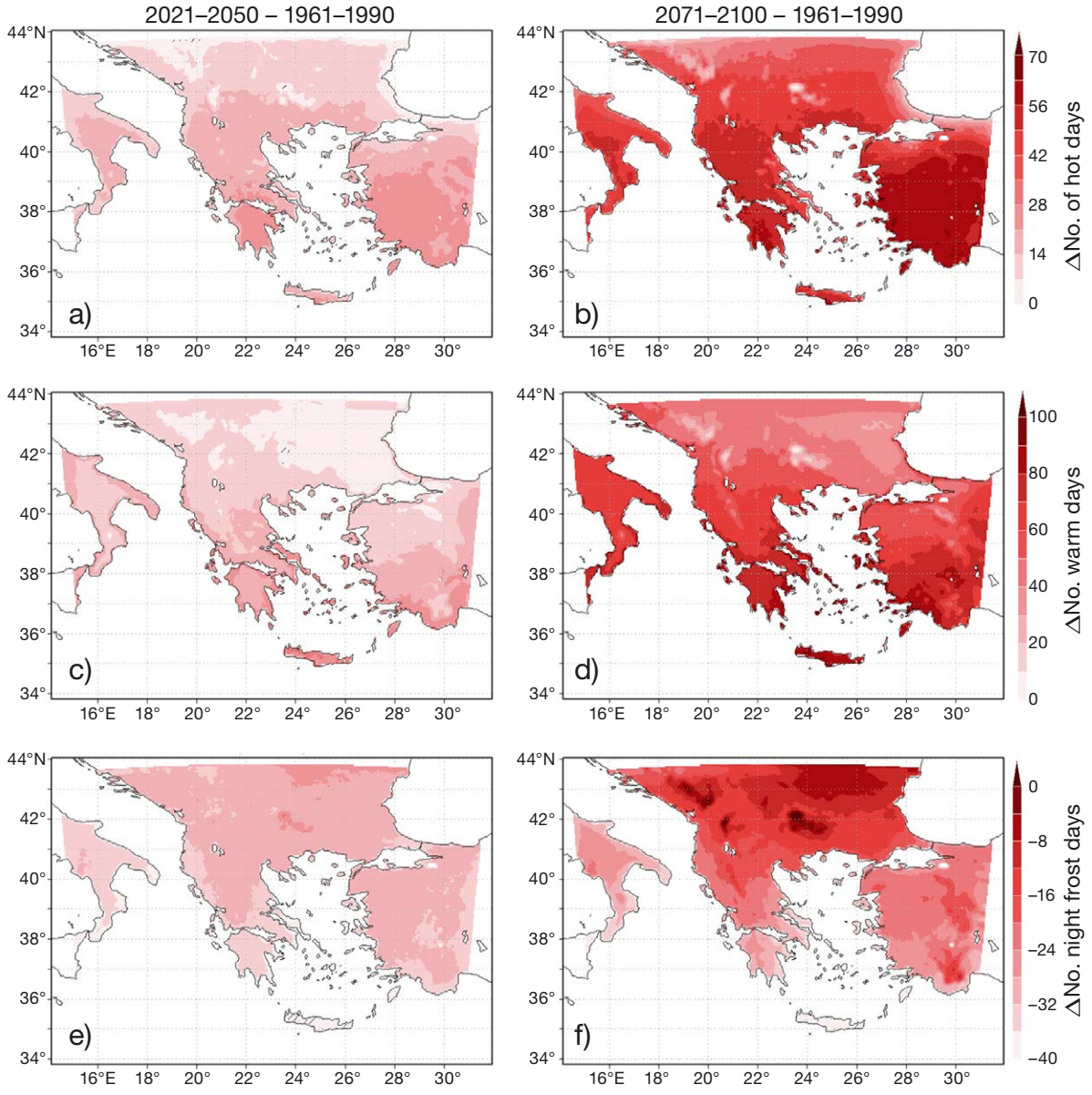


Fig. 9. Annual change between 2021–2050 and 1961–1990 as well as between 2071–2100 and 1961–1990 for (a,b) the number of hot days with Tmax > 35°C, (c,d) the number of warm with days with Tmin > 20°C and (e,f) the number of night frost days with Tmin < 0°C based on the high-resolution simulation RCM10. All differences are statistically significant at the 95% confidence level according to a 2-tailed paired *t*-test

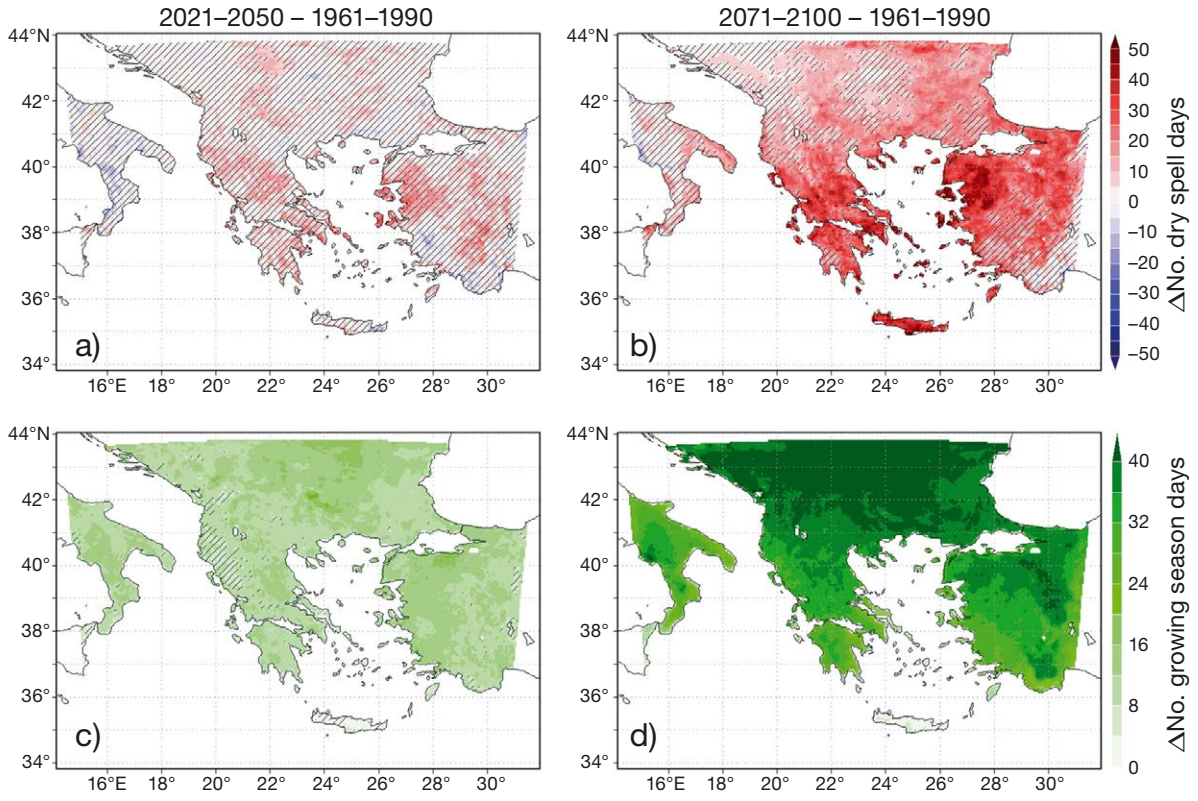


Fig. 10. Similar to Fig. 9 but for (a,b) dry spell days and (c,d) growing season days. The line shading indicates areas in which the differences between future runs and the control run are not statistically significant at the 95% confidence level according to a 2-tailed paired *t*-test

Finally, concerning the number of continuous dry spell days with daily precipitation < 1 mm, there is a tendency for an increase of about 5 to 20 d for the FUT1 period in most parts of northwestern, central and southern Greece, but there are areas with no change in northern Greece (e.g. central and eastern Macedonia) or with even a small decrease such as in northeastern Greece (Thrace) and Crete (Fig. 10a). This is consistent with the pattern of precipitation changes in the FUT1 period (Fig. 6a). In the FUT2 period, a general increase in the number of continuous dry spell days in the range of 10 to 40 d is projected for the majority of Greece due to the anticipated overall reduction in precipitation (Fig. 10b). Furthermore, increases in the number of continuous dry spell days are higher over southern Greece than over northern Greece in accordance with the pattern of precipitation changes in the FUT2 period (Fig. 6b).

## 4. DISCUSSION AND CONCLUSIONS

A high-resolution simulation (RCM10) was carried out with RegCM3 over the period 1960–2100 under the A1B scenario, which is a transient regional projection for future climate change, for the first time to our knowledge with 10 km spatial resolution for Greece. Based on a previous study for optimisation of the model configuration concerning the convection scheme (Mystakidis et al. 2012), the RCM10 simulation was performed using the Emanuel scheme with modified parameters in the rate at which the cloud-base upward mass flux is relaxed to steady state, and in the warm cloud autoconversion threshold.

The RCM10 simulation was evaluated over the period 1975–2000 using temperature and precipitation measurements from 79 stations of the HNMS observational network. Selection of the period 1975–2000 was based on optimum spatial coverage of stations over this period. RCM10 precipitation and temperature fields depict the finer regional characteristics over the complex Greek terrain compared to RCM25. However, the station-based evaluation does not reveal a considerable improvement in RCM10 compared to RCM25, with only a slight reduction in the annual bias in near-surface temperature and precipitation over mountain regions, presumably related to the different convective schemes implemented through a feedback mechanism, as has also been discussed by Zanis et al. (2009b) and Mystakidis et al.

(2012). The higher spatial resolution in RCM10 versus RCM25 does not lead to improvements of the temporal and spatial correlations of temperature and precipitation, presumably because of the limited number of stations over the mountainous regions, and the complex terrain. The projected changes in mean annual near-surface temperature for the near-future period (2021–2050) are in the range of up to 1.4°C over central and northern Greece to up to 1.8°C over parts of Peloponnese and Crete as well as islands of the Aegean Sea. Concerning precipitation, the near-future changes are statistically non-significant at the 95% confidence level. At the end of the 21st century, larger changes in both near-surface temperature and precipitation are projected, with mean annual temperature increasing by about 3.4 to 4.2°C over land and by 2.6 to 3.4°C over the sea and precipitation decreasing by 10 to 40%, with a positive gradient from the north to the south. As has been discussed in Tolika et al. (2012), the different sea–land warming, with a maximum in summer, could be attributed to the differences in heat capacity and evaporation of the sea water. These RCM10 simulated changes in annual temperature and precipitation are in accordance with a regional climate change ensemble from the ENSEMBLES project under the A1B scenario indicating a temperature increase over the inland area of Greece of about 3.5 to 4.0°C and precipitation decrease of about 15 to 25% (Jacob et al. 2014). Furthermore, the recent high-resolution climate change ensemble from the EURO-CORDEX initiative indicated a temperature increase over the inland area of Greece of about 2 to 2.5°C and a small precipitation decrease up to15% in southern Greece for the RCP4.5 scenario, while RCP8.5 indicated a temperature increase of about 4 to 5°C and a precipitation decrease of 5 to 35% (Jacob et al. 2014).

The future projected climate change signal in the RCM10 simulation is also in agreement with previous model simulations based on RCMs indicating a consistent warming and drying of the Mediterranean region mainly over the last decades of the 21st century for various emission scenarios (e.g. Gibelin & Déqué 2003, Gao et al. 2006, Diffenbaugh et al. 2007, Goubanova & Li 2007, Giorgi & Lionello 2008, Önol & Semazzi 2009, Krichak et al. 2011, Lelieveld et al. 2013). The simulated RCM25 projected changes in near-surface temperature and precipitation are similar to RCM10 in magnitude and spatial distribution, indicating the robustness of the RegCM future projections, despite the different resolution and the different convective schemes implemented.

Future changes in maximum annual temperature are slightly higher, and changes in minimum annual temperature are slightly lower, when compared to the changes in mean annual temperature. Similar results showing higher sensitivity of Tmax than Tmin in future climate projections for the Mediterranean have also been reported in previous studies based on both GCMs and RCMs (Sánchez et al. 2004, Lobell et al. 2007, Elguindi et al. 2013). This could be linked to drying and its impacts on Tmax during the warm period of the year through decreases in cloud cover and the surface latent heat flux (Dai et al. 2004, van der Schrier et al. 2006), pointing also to the role of soil moisture depletion in the amplification of climate warming in the EM (Zittis et al. 2014).

The largest seasonal changes in mean near-surface temperature are seen during summer over the Greek mainland, with values in the late 21st century from 3.8 to 4.6°C for southern Greece, 4.6 to 5°C for northeastern Greece and >5°C for northwestern Greece. These simulated changes in summer mean near-surface temperature are in agreement with the study of Tolika et al. (2012) that reported changes in the range of 4 to 5.5°C for Greece from an ensemble of 8 RCMs under the A1B scenario. The changes in maximum near-surface temperature in summer for FUT2 are slightly higher, with values >5°C covering a large part of northern Greece, possibly related to the winter and spring drying over the same regions and the soil moisture–temperature feedback discussed by Zittis et al. (2014). These RCM10 projected summertime changes in Tmax are in the range of simulated Tmax changes with the PRECIS model under A1B for the EM (Lelieveld et al. 2013). Lelieveld et al. (2013) reported that across the Balkan Peninsula and Turkey, climate change is particularly rapid, and temperatures, especially in summer, are expected to increase strongly. Concerning seasonal precipitation changes in the late 21st century, winter shows the largest decreases in precipitation rate in western and southern Greece, while spring shows the largest decreases in northern Greece. The simulated decrease in precipitation in winter over the Mediterranean (especially at the end of the 21st century) is linked to an increase in the sea level pressure (SLP) gradient between the Azores High and the Icelandic Low that results in an intensified zonal circulation over Europe and a northward shift of the location of the storm tracks, which in turn leads to more precipitation in central Europe and less precipitation in southern Europe. This is a common finding in many GCM and RCM simulations for the area of interest (Giorgi & Lionello 2008, Tolika et al. 2012). The summer drying

over the area of interest is probably associated with the SLP increase over the British Isles and western Europe, leading to weakening of the westerly flow, while a less significant soil moisture–precipitation feedback due to soil moisture depletion is expected to further amplify the dryer and warmer conditions over the domain of the study (Seneviratne et al. 2006, Zanis et al. 2009b, Zittis et al. 2014). Also, the model's SLP decrease over the Mediterranean is probably a result of the intense temperature increase and is consistent with a weakening and poleward expansion of the Hadley circulation in the climate change simulations of the IPCC AR4 project (Lu et al. 2007).

The number of hot days, warm nights and night frost days and the length of the growing season are projected to increase in the near- and late-future periods in accordance with the generally warmer climate projected from the RCM10 simulation for Greece. Furthermore, there is a tendency for a slight increase in the number of continuous dry spell days in the near-future period in most parts of northwestern, central and southern Greece (but not for north central and northeastern Greece), while in the late 21st century, a general increase is projected for the whole of Greece in accordance with the projected overall reduction in precipitation. The reported future climatic changes based on this high-resolution RCM simulation could be a valuable dataset for other researchers for the study of impacts in vital sectors such as water resources, agriculture, tourism, forest fire risk and energy demand for the region of Greece.

*Acknowledgements.* The research was co-financed by the European Union (European Regional Development Fund) and Greek national funds through the Operational Program 'Competitiveness and Entrepreneurship' of the National Strategic Reference Framework (NSRF)–Research Funding Program COOPERATION 2009 (no. 09SYN-31-1094, 'Development of a Geographic Climate Information System'). The RCM25 simulations over Europe, used as lateral boundary conditions for our RCM10 simulations, were provided by the Earth System Physics section of the International Centre for Theoretical Physics (ICTP), Trieste, Italy, and we acknowledge support by Filippo Giorgi and Erika Coppola from ICTP. The high-resolution regional climate simulations were performed in the EGI/HellasGrid infrastructure. We acknowledge the E-OBS dataset from the EU-FP6 project ENSEMBLES (http://ensembles-eu.metoffice.com), data providers in the ECA&D project (www.ecad.eu), and the forcing GCM ECHAM5 r3 download from the CERA database (http://cera-www.dkrz.de/CERA/index.html). Finally, we thank the reviewers for their constructive comments.

## LITERATURE CITED

Christensen JH, Christensen OB (2007) A summary of the PRUDENCE model projections of changes in European climate by the end of this century. Clim Change 81:7–30

Crétat J, Pohl B (2012) How physical parameterizations can modulate internal variability in a regional climate model. J Atmos Sci 69:714–724

Dai A, Trenberth K, Qian T (2004) A global dataset of Palmer drought severity index for 1870–2002: relationship with soil moisture and effects of surface warming. J Hydrometeorol 5:1117–1130

Déqué M, Rowell DP, Lüthi D, Giorgi F and others (2007) An intercomparison of regional climate simulations for Europe: assessing uncertainties in model projections. Clim Change 81:53–70

Dickinson R, Errico R, Giorgi F, Bates G (1989) A regional climate model for the western United States. Clim Change 15:383–422

Dickinson R, Henderson-Sellers A, Kennedy PJ (1993) Biosphere–Atmosphere Transfer Scheme, BATS: version 1E as coupled to the NCAR community climate model. Tech Note NCAR/TN-387+STR, National Center for Atmospheric Research, Boulder, CO

Diffenbaugh NS, Pal JS, Giorgi F, Gao X (2007) Heat stress intensification in the Mediterranean climate change hotspot. Geophys Res Lett 34:L11706, doi:10.1029/2007GL030000

Elguindi N, Rauscher SA, Giorgi F (2013) Historical and future changes in maximum and minimum temperature records over Europe. Clim Change 117:415–431

Emanuel KA, Živkovi -Rothman M (1999) Development and evaluation of a convection scheme for use in climate models. J Atmos Sci 56:1766–1782

Fritsch JM, Chappell CF (1980) Numerical prediction of convectively driven mesoscale pressure systems. I. Convective parameterization. J Atmos Sci 37:1722–1733

Gao X, Pal JS, Giorgi F (2006) Projected changes in mean and extreme precipitation over the Mediterranean region from a high resolution double nested RCM simulation. Geophys Res Lett 33:L03706, doi:10.1029/2005GL024954

Gibelin AL, Déqué M (2003) Anthropogenic climate change over the Mediterranean region simulated by a global variable resolution model. Clim Dyn 20:327–339

Giorgi F (2006) Climate change hot-spots. Geophys Res Lett 33:L08707, doi:10.1029/2006GL025734

Giorgi F, Pal JS, Bi XQ, Sloan LC, Elguindi N, Solmon F (2006) Introduction to the TAC special issue: the RegCNET network. Theor Appl Climatol 86:1–4

Giorgi F, Bi X (2000) A study of internal variability of a regional climate model. J Geophys Res 105:29503–29521

Giorgi F, Lionello P (2008) Climate change projections for the Mediterranean region. Global Planet Change 63: 90–104

Giorgi F, Mearns LO (1999) Introduction to special section: regional climate modeling revisited. J Geophys Res 104: 6335–6352

Giorgi F, Marinucci MR, Visconti G (1990) Use of a limited-area model nested in a general circulation model for regional climate simulation over Europe. J Geophys Res Atmos 95:18413–18431

Giorgi F, Bi X, Pal J (2004) Mean, interannual variability and trends in a regional climate change experiment over Europe. II. Climate change scenarios (2071–2100). Clim Dyn 23:839–858

Goubanova K, Li L (2007) Extremes in temperature and precipitation around the Mediterranean basin in an ensemble of future climate scenario simulations. Global Planet Change 57:27–42

Grell GA (1993) Prognostic evaluation of assumptions used by cumulus parameterizations. Mon Weather Rev 121: 764–787

Grell GA, Dudhia J, Stauer DR (1994) A description of the fifth-generation Penn State/NCAR mesoscale model (mm5). Tech Note NCAR/TN-398+STR, National Center for Atmospheric Research, Boulder, CO

Hadjinicolaou P, Giannakopoulos C, Zerefos C, Lange MA, Pashiardis S, Lelieveld J (2011) Mid-21st century climate and weather extremes in Cyprus as projected by six regional climate models. Reg Environ Change 11: 441–457

Haylock MR, Hofstra N, Klein Tank AMG, Klok EJ, Jones PD, New M (2008) A European daily high-resolution gridded data set of surface temperature and precipitation for 1950–2006. J Geophys Res 113:D20119, doi:10.1029/2008JD010201

Held I, Zhao M (2011) The response of tropical cyclone statistics to an increase in $CO_2$ with fixed sea surface temperatures. J Clim 24:5353–5364

Holtslag AAM, de Bruijn EIF, Pan HL (1990) A high resolution air mass transformation model for short-range weather forecasting. Mon Weather Rev 118:1561–1575

Im ES, Coppola E, Giorgi F, Bi X (2010) Validation of a high resolution regional climate model for the Alpine region and effects of a subgrid-scale topography and land use representation. J Clim 23:1854–1873

IPCC (2007) Climate change 2007: the physical science basis. In: Solomon S, Qin D, Manning M, Chen Z and others (eds) Contribution of Working Group I to the Fourth Assessment Report of the Intergovernmental Panel on Climate Change, Cambridge University Press, Cambridge

Jacob D, Bärring L, Christensen OB, Christensen JH and others (2007) An inter-comparison of regional climate models for Europe: model performance in present-day climate. Clim Change 81:31–52

Jacob D, Petersen J, Eggert B, Alias A and others (2014) EURO-CORDEX: new high-resolution climate change projections for European impact research. Reg Environ Change 14:563–578

Kiehl JT, Hack JJ, Bonan GB, Boville BA, Breigleb BP, Williamson D, Rasch P (1996) Description of the NCAR community climate model (ccm3). Tech Note NCAR/TN-420+STR, National Center for Atmospheric Research, Boulder, CO

Kostopoulou E, Giannakopoulos C, Anagnostopoulou C, Tolika K, Maheras P, Vafiadis M, Founda D (2007) Simulating maximum and minimum temperature over Greece: a comparison of three downscaling techniques. Theor Appl Climatol 90:65–82

Krichak SO, Breitgand JS, Samuels R, Alpert P (2011) A double-resolution transient RCM climate change simulation experiment for near-coastal eastern zone of the eastern Mediterranean region. Theor Appl Climatol 103:167–195

Laprise R, de Elía R, Caya D, Biner S and others (2008) Challenging some tenets of regional climate modelling. Meteorol Atmos Phys 100:3–22

Lelieveld J, Hadjinicolaou P, Kostopoulou E, Giannakopoulos C, Pozzer A, Tanarhte M, Tyrlis E (2013) Model projected heat extremes and air pollution in the eastern Mediterranean and Middle East in the twenty-first century. Reg Environ Change 14:1937–1949

Lobell DB, Bonfils C, Duffy PB (2007) Climate change uncertainty for daily minimum and maximum temperatures: a model inter-comparison. Geophys Res Lett 34:L05715, doi:10.1029/2006GL028726

Lu J, Vecchi GA, Reichler T (2007) Expansion of the Hadley cell under global warming. Geophys Res Lett 34:L06805, doi:10.1029/2006GL028443

Maheras P, Flocas HA, Patrikas I, Anagnostopoulou C (2001) A 40 year objective climatology of surface cyclones in the Mediterranean region: spatial and temporal distribution. Int J Climatol 21:109–130

Maheras P, Anagnostopoulou C (2003) Circulation types and their influence on the interannual variability and precipitation changes in Greece. In: Bolle HJ (ed) Mediterranean climate: variability and trends. Springer, Berlin, p 215–239

Marougianni G, Melas D, Kioutsioukis I, Feidas H, Zanis P, Anadranistakis E (2012) Trend analysis for climatic time series for Greece. In: Helmis CG, Nastos PT (eds) Advances in meteorology, climatology and atmospheric physics. Springer, Berlin, p 583–589

Meinshausen M, Smith SJ, Calvin K, Daniel JS and others (2011) The RCP greenhouse gas concentrations and their extensions from 1765 to 2300. Clim Change 109:213–241

Mystakidis S, Zanis P, Dogras C, Katragkou E and others (2012) Optimization of a regional climate model for high resolution simulations over Greece. In: Helmis CG, Nastos PT (eds) Advances in meteorology, climatology and atmospheric physics. Springer, Berlin, p 623–629

Nastos PT, Politi N, Kapsomenakis J (2013) Spatial and temporal variability of the aridity index in Greece. Atmos Res 119:140–152

O'Brien TA, Sloan LC, Snyder MA (2011) Can ensembles of regional climate model simulations improve results from sensitivity studies? Clim Dyn 37:1111–1118

Önol B (2012) Effects of coastal topography on climate: high-resolution simulation with a regional climate model. Clim Res 52:159–174

Önol B, Semazzi FHM (2009) Regionalization of climate change simulations over the eastern Mediterranean. J Clim 22:1944–1961

Pal JS, Small EE, Eltahir EAB (2000) Simulation of regional-scale water and energy budgets: representation of subgrid cloud and precipitation processes within RegCM. J Geophys Res 105:29579–29594

Pal JS, Giorgi F, Bi X, Elguindi N and others (2007) Regional climate modeling for the developing world: the ICTP RegCM3 and RegCNET. Bull Am Meteorol Soc 88: 1395–1409

Rauscher S, Coppola E, Piani C, Giorgi F (2010) Resolution effects on regional climate model simulations of seasonal precipitation over Europe. Clim Dyn 35:685–711

Rodwell MJ, Hoskins BJ (1996) Monsoons and the dynamics of deserts. QJR Meteorol Soc 122:1385–1404

Roeckner E (2006) ENSEMBLES ECHAM5-MPI-OM 20C3M run1, monthly mean values. CERA database. World Data Center for Climate, Hamburg. Available at: http://cera-www.dkrz.de/WDCC/ui/Compact.jsp?acronym=ENSEMBLES_MPEH5_20C3M_1_MM

Roeckner E (2008) ENSEMBLES ECHAM5-MPI-OM SRESA1B run3, monthly mean values. CERA database. World Data Center for Climate, Hamburg. Available at: http://cera-www.dkrz.de/WDCC/ui/Compact.jsp?acronym=ENSEMBLES_MPEH5_SRA1B_3_MM

Rogelj J, Meinshausen M, Knutti R (2012) Global warming under old and new scenarios using IPCC climate sensitivity range estimates. Nat Clim Change 2:248–253

Sánchez E, Gallardo C, Gaertner MA, Arribas A, Castro M

(2004) Future climate extreme events in the Mediterranean simulated by a regional climate model: a first approach. Global Planet Change 44:163–180

Sanchez-Gomez E, Somot S, Déqué M (2009) Ability of an ensemble of regional climate models to reproduce weather regimes over Europe-Atlantic during the period 1961–2000. Clim Dyn 33:723–736

Segele ZT, Leslie LM, Lamb PJ (2009) Evaluation and adaptation of a regional climate model for the Horn of Africa: rainfall climatology and interannual variability. Int J Climatol 29:47–65

Seneviratne SI, Lüthi D, Litschi M, Schär C (2006) Land-atmosphere coupling and climate change in Europe. Nature 443:205–209

Tolika K, Anagnostopoulou C, Maheras P, Vafiadis M (2008) Simulation of future changes in extreme rainfall and temperature conditions over the Greek area: a comparison of two statistical downscaling approaches. Global Planet Change 63:132–151

Tolika K, Zanis P, Anagnostopoulou C (2012) Regional climate change scenarios for Greece: future temperature and precipitation projections from ensembles of RCMs. Global NEST J 14:407–421

Torma C, Coppola E, Giorgi F, Bartholy J, Pongrácz R (2011) Validation of a high-resolution version of the regional climate model RegCM3 over the Carpathian Basin. J Hydrometeorol 12:84–100

Tselioudis G, Douvis C, Zerefos C (2012) Does dynamical downscaling introduce novel information in climate model simulations of precipitation change over a complex topography region? Int J Climatol 32:1572–1578

Tyrlis E, Lelieveld J, Steil B (2013) The summer circulation over the eastern Mediterranean and the Middle East: influence of the South Asian monsoon. Clim Dyn 40: 1103–1123

van der Schrier G, Briffa KR, Jones PD, Osborn TJ (2006) Summer moisture variability across Europe. J Clim 19: 2818–2834

Xoplaki E, González-Rouco JF, Luterbacher J, Wanner H (2004) Wet season Mediterranean precipitation variability: influence of large-scale dynamics and trends. Clim Dyn 23:63–78

Xue Y, Janjic Z, Dudhia J, Vasic R, De Sales F (2014) A review on regional dynamical downscaling in intraseasonal to seasonal simulation/prediction and major factors that affect downscaling ability. Atmos Res 147–148: 68–85

Zanis P, Douvis C, Kapsomenakis I, Kioutsioukis I, Melas D, Pal JS (2009a) A sensitivity study of the regional climate model (RegCM3) to the convective scheme with emphasis in central eastern and southeastern Europe. Theor Appl Climatol 97:327–337

Zanis P, Kapsomenakis I, Philandras C, Douvis K and others (2009b) Analysis of an ensemble of present day and future regional climate simulations for Greece. Int J Climatol 29:1614–1633

Zerefos C, Repapis C, Giannakopoulos C, Kapsomenakis J and others (2011) The climate of the eastern Mediterranean and Greece: past, present and future. In: The environmental, economic and social impacts of climate change in Greece. Climate Change Impacts Study Committee, Bank of Greece, Athens, p 1–126

Zittis G, Hadjinicolaou P, Lelieveld J (2014) Role of soil moisture in the amplification of climate warming in the eastern Mediterranean and the Middle East. Clim Res 59: 27–37

*Editorial responsibility: Filippo Giorgi, Trieste, Italy*

*Submitted: September 10, 2014; Accepted: April 20, 2015*
*Proofs received from author(s): July 2, 2015*